Enhancement of PAB3D for Unsteady Simulations

Steven J. Massey
Eagle Aeronautics, Inc.
Hampton, VA

Khaled S. Abdol-Hamid
Analytical Services and Materials, Inc.
Hampton, VA

October, 2001

1 Introduction

Investigations in the area of unsteady flow control for propulsion applications have led to an increased interest in upgrading PAB3D's time accurate capabilities. PAB3D is a structured, multiblock, parallel, implicit, finite-volume solver, of the three-dimensional, unsteady, Reynolds-averaged Navier-Stokes equations. Advanced turbulence models are available and are widely used in internal and external flow applications by NASA and the US aerospace industry. In recognition of the importance of the continued enhancement of the PAB3D solver for use in industry and government projects, the NASA Langley Research Center has advocated the long-term development of the code. The present addition of improved algorithms for second-order time accuracy, sub-iteration schemes and unsteady jet boundary conditions provide key modernizing enhancements to the code. In this task, two widely used time advancement schemes [1–3] are implemented in PAB3D and validated against experimental data [4–6].

2 Time Advancement Formulation

The flux vector form of the Navier-Stokes equations may be written in indicial notation as

$$\frac{1}{J}\frac{\partial \mathbf{Q}}{\partial t} = -\frac{\partial}{\partial \xi_j}\left[\mathbf{E}_j - (\mathbf{E}_v)_j\right] = \mathbf{R}(\mathbf{Q}) \tag{1}$$

where $\mathbf{Q}$ is the flow vector, $\mathbf{E}_j$ and $(\mathbf{E}_v)_j$ are the j^{th} inviscid and viscous flux vectors respectively and $\mathbf{R}$ is the residual vector. The time dependent term may be discretized with backward differencing as

$$\frac{(1+\phi)(\mathbf{Q}^{n+1} - \mathbf{Q}^{n}) - \phi(\mathbf{Q}^{n} - \mathbf{Q}^{n-1})}{J\Delta t} = \mathbf{R}(\mathbf{Q}^{n+1}) \tag{2}$$

and rearranging Eq. (2) gives

$$\frac{(1+\phi)}{J\Delta t}(\mathbf{Q}^{n+1} - \mathbf{Q}^{n}) = \mathbf{R}(\mathbf{Q}^{n+1}) + \frac{\phi(\mathbf{Q}^{n} - \mathbf{Q}^{n-1})}{J\Delta t} \tag{3}$$

where the superscripts indicate the time level, and $\phi = 0$ and $\phi = \frac{1}{2}$ result in a first or second-order time accurate difference respectively. As a means of improving time accuracy, two sub-iteration schemes are implemented, duel or pseudo time stepping and physical time stepping. In duel time sub-iterations, the time step is allowed to vary across all cells based on a constant CFL. In physical time sub-iteration the time step is constant for all cells. For the duel time scheme, an additional pseudo time term is added to Eq. (2),

$$\frac{\mathbf{Q}^{m+1} - \mathbf{Q}^{m}}{J\Delta\tau} + \frac{(1+\phi)(\mathbf{Q}^{m+1} - \mathbf{Q}^{n})}{J\Delta t} = \mathbf{R}(\mathbf{Q}^{m+1}) + \frac{\phi(\mathbf{Q}^{n} - \mathbf{Q}^{n-1})}{J\Delta t} \tag{4}$$

and rearranging Eq. (4) gives

$$\left[\frac{1}{J\Delta\tau} + \frac{(1+\phi)}{J\Delta t}\right](\mathbf{Q}^{m+1} - \mathbf{Q}^{m}) = \mathbf{R}(\mathbf{Q}^{m+1}) + \frac{\phi(\mathbf{Q}^{n} - \mathbf{Q}^{n-1})}{J\Delta t} - \frac{(1+\phi)(\mathbf{Q}^{m} - \mathbf{Q}^{n})}{J\Delta t} \tag{5}$$

where m is the sub-iteration index and $\Delta\tau$ represents the pseudo time step. As $m \rightarrow \infty$, the pseudo term vanishes and with convergence $\mathbf{Q}^{m+1} \rightarrow \mathbf{Q}^{n+1}$. To generalize the time accurate scheme for any of the implicit formulations in PAB3D, $\mathbf{R}(\mathbf{Q})$ is linearized and the RHS is rewritten as,

$$RHS = \mathbf{R}(\mathbf{Q}^{m}) + \frac{\phi(\mathbf{Q}^{n} - \mathbf{Q}^{n-1})}{J\Delta t} - \frac{(1+\phi)(\mathbf{Q}^{m} - \mathbf{Q}^{n})}{J\Delta t} \tag{6}$$

Additionally, the time step in the implicit side is replaced by

$$\frac{1}{J\Delta t_{imp}} = \left[\frac{1}{J\Delta\tau} + \frac{(1+\phi)}{J\Delta t}\right] \tag{7}$$

where the quantity $\Delta\tau$ is set accourding to a constant CFL number. The physical time sub-iteration scheme is similar to the duel time stepping method with the exception that the implicit time step term is now defined as

$$\frac{1}{J\Delta t_{imp}} = \left[\frac{(1+\phi)}{J\Delta t}\right] \tag{8}$$

2.1 Usage

The interface to the new time accurate features reside on a new segment of the `user.cont`, an example and definitions are given as follows:

```
'Begin TimeStep Cont'
ir0  ratr ita cfltau ncycle
  1  0.10  -2     5.      5
'End TimeStep Cont'
```

Variable	**Value**	**Definition**
`ir0`	0*	Residual calculated from l_2 norm of $\mathbf{Q}$ over all cells
	1	Residual calculated from l_2 norm of ρ over all cells
`ratr`	0.5*	Limiter factor based on ρ per time step and imposed on $\mathbf{Q}$

`ita`	1*	First-order time accuracy with physical time sub-iteration
	2	Second-order time accuracy with physical time sub-iteration
	-1	First-order time accuracy with duel time sub-iteration
	-2	Second-order time accuracy with duel time sub-iteration
`cfltau`		CFL number for duel time sub-iteration
`ncycle`		Number of time iterations per physical time level, ie. `ncycle`=1 for no sub-iterations. Typical value is 5, which gives 4 sub-iterations.

where (*) denotes the default value used when the `TimeStep` segment is omitted. The constant global time step is calculated from the CFL of the smallest cell, provided by the `dt` input in `tpab3d.cont`. Note, that `dt < 0` indicates the CFL per grid cell is constant for pseudo time stepping. To obtain the actual time step used for time accurate calculations, see the `PAB.out` file, for example:

```
 Time Accurate Procedure
 dtmin=   2.3720261E-08 dtmax=   4.9344753E-06 CFLM=    100.0000
 time step in secs   2.3720261E-06
 normalized time step    8.0963218E-04
 Actual CFL =    100.0000
```

3 Unsteady Jet Boundary Conditions

A set of generalized, harmonic, jet boundary conditions for total pressure and velocity is provided. In addition, skeleton routines are provided for user supplied boundary conditions. The boundary conditions are implemented as a generalization of the existing constant total values and constant static values boundary conditions, `ibcijk` = -22 and -23 respectively, where the constant values now represent the datum.

3.1 Total Pressure

The form of the built-in oscillatory jet boundary condition for total pressure is

$$p_t = p_{t_0}[1 + A\cos(2\pi\omega t + \phi)] \tag{9}$$

where p_{t_0} is the steady state value, A is the amplitude, ω is the frequency in Hertz and ϕ is the phase shift angle in degrees. These values are supplied through an extension of the existing constant total pressure boundary condition (`ibcijk=-22`). Input data is supplied in the `Surf Cont` segment of the `user.cont` file. For example:

```
'Begin Surf Cont'
 iblk iface icut iunit n_x n_y n_z  Mach   P_s   T_s     amp     freq phase ifun
    9     3    1     0   0   0    1 0.723 13.81 905.45 0.1667 210.7908   90.    0
'End Surf Cont'
```

where the variables are defined as follows:

Variable	Value	Definition
iblk, iface, icut		Block, face and cut address of boundary condition
iunit	0	American units (psi, Rankine)
	1	SI units, (Pa, Kelvin)
n_x, n_y, n_z		Unit velocity vector of jet
Mach		Mach number of jet
P_s		Static pressure of jet
T_s		Static temperature of jet
amp		Amplitude, $0 \leq A < 1$
freq		Frequency, ω [Hz]
phase		Phase shift angle, ϕ [deg]
ifun	0	Built in harmonic function
	1	User function u_pressure_1
	2	User function u_pressure_2
	3	User function u_pressure_3
	4	User function u_pressure_4

An equivalent user function to the standard harmonic total pressure function is coded as an example:

```
function u_pressure_1(t,amp,freq,phase)
parameter(pi2=6.28318507)
u_pressure_1 = amp*cos(freq*t*pi2+phase)
return
end
```

where only the unsteady portion of Eq. (9) is coded. Here t is the absolute physical time value and phase has already been converted to radians on reading on input. The function is located in src/Pab3/user.F

3.2 Velocity

The form of the built-in oscillatory jet boundary condition for velocity is

$$\mathbf{V} = \mathbf{V}_0[1 + A\cos(2\pi\omega t + \phi)] \tag{10}$$

where $\mathbf{V}_0$ is the steady state value obtained from the unit flow vector (n_x, n_y, n_z) and Mach number input. These values are supplied through an extension of the existing constant static values boundary condition (ibcijk=-23). Input data is supplied as discussed above for the total pressure boundary condition, with the exception that ifun=0 triggers the default velocity function and ifun=1,2,3 or 4 now calls one of the four user supplied velocity functions, u_vel_1 etc., which are located in src/Pab3/user.F . The form of the user supplied velocity functions is similar to the total pressure implementation, where only the unsteady term is assigned to the Fortran function, ie. Eq.(10) becomes

$$\mathbf{V} = \mathbf{V}_0[1 + \texttt{u\_vel\_1}] \tag{11}$$

Table 1: Circular Cylinder: Strouhal number results

Re	1st-order	2nd-order, duel	2nd-order, physical	Experiment
100		0.160		0.160-0.170
200	0.175	0.182	0.196	0.180-0.200
1000		0.198	0.225	0.195-0.215
10000		0.200	0.240	0.190-0.205
90000		0.207		0.185-0.200

4 Results

Two geometries are examined to validate the new features of the code. To validate the time accuracy of the code, the well known case of the circular cylinder in cross-flow is solved and the vortex shedding frequency is compared with experimental results. To demonstrate the new oscillatory jet boundary condition, a 3D jet is cross-flow is simulated.

4.1 Circular Cylinder in Cross-flow

The frequency with which vortices are shed in a Kármàn vortex street behind a circular cylinder has been studied in numerous experiments [4–6], from which a range of dimensionless frequency or Strouhal number is tabulated along with CFD results, 4.1. Strouhal number is defined as

$$St = \frac{nD}{V} \tag{12}$$

where n is the dimensional frequency, D is the cylinder diameter and V is the free-stream velocity.

The flow field around the cylinder is simulated by solving the unsteady, compressible, laminar Navier-Stokes equations using an implicit, up-wind, flux-difference splitting, finite volume scheme. Turbulence is not modeled, due to the uncertain time accuracy of the models and the fact that all but the highest Reynolds number case is well below the $Re_{crit} \approx 30,000$ [6]. The 2D grid consisted of 34,832 cells and 6 blocks, and extended 20 diameters into the far-field, see Figure 1. The same grid was used for all runs, which gave a maximum y^+ range of approximately 0.04 to 17. The shedding frequencies are observed from the pressure contribution of lift, which is obtained via internal *Post* stream thrust function integrated over the solid surface. A sample contour plot of Mach number showing the vortex street is shown in Figure 2.

For the second-order time accurate cases, it was observed that approximately five time iterations per physical time step produced the optimal convergence per iteration. However, the physics of the specific problem will dictate this number for other cases. In the present results, five iterations typically reduced the residual by three orders of magnitude at that time level. The first-order time accurate case was run with no sub-iterations, to be consistent with the earlier PAB3D version. The solution strategy for this case is to first run at coarse grid level and large time step to trigger the vortex shedding instability, then refine the grid and time step for accuracy. The onset, coarse grid - large time step, and fine grid - small time step portions of the solution process can easily been seen in the C_L history plots for the three time integration schemes, Figures 3- 5 for $Re = 200$. The physical time iteration scheme, showed the most consistent amplitude and frequency for C_L between coarse and fine solutions for $Re = 200$. However, tabulated results for higher Re, Table 4.1, show the physical time scheme to over predict the shedding frequency, St. Further study is required to isolate the causes for this deviation.

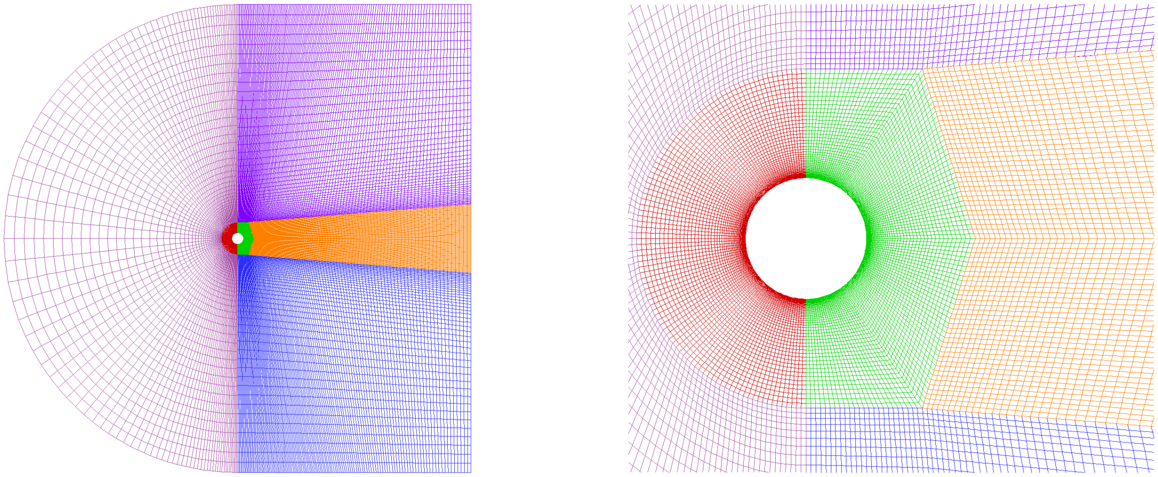

Figure 1: Circular Cylinder: Far and near field grid

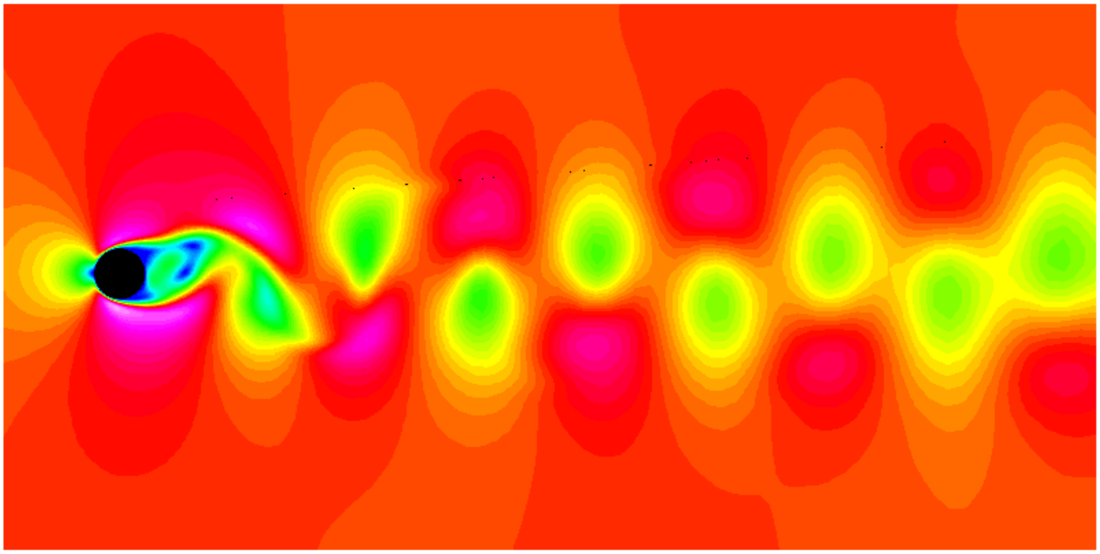

Figure 2: Circular Cylinder: Mach contours, $Re = 200$, second-order, duel time solution.

4.2 3D Oscillating Jet in Cross-flow

To demonstrate the new oscillatory jet boundary condition, a 3D jet is cross-flow is simulated. Only results for the total pressure boundary condition are presented. The velocity condition was tested for correctness but was not used in a full simulation. The geometry and

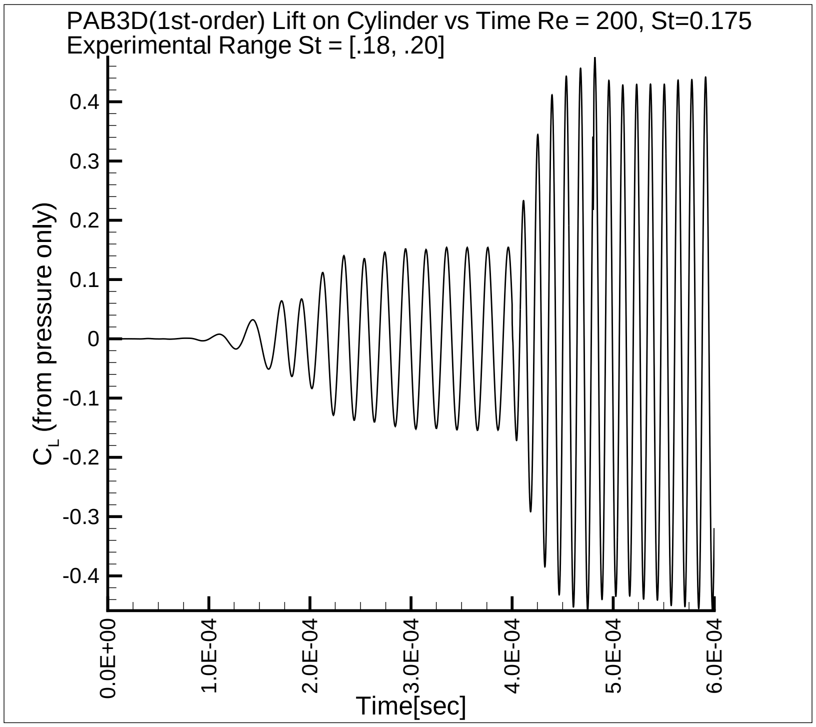

Figure 3: Circular Cylinder: C_L history, first-order time accurate

flow conditions are chosen arbitrarily and have a length, width and jet radius of 30cm, 3cm and 3mm respectively. The grid consisted of 9 blocks totaling 308,736 cells, see Figures 6 and 7. The fluid flow is simulated by solving the unsteady, compressible, Reynolds-averaged Navier-Stokes equations using an implicit, up-wind, flux-difference splitting, finite volume scheme and standard two equation $k-\varepsilon$ turbulence model with a linear stress representation. Uncoupled viscous terms are retained in all directions. A four step process is used to accelerate convergence by first solving half of the grid in each of the three computational directions for approximately 3000 iterations, then solving the finer grid for another 3000 iterations. For the first to steps, the steady state solution is obtained from running in pseudo time stepping. To insure there are no non-physical unsteady flow features in the baseline flow, another 1000 iterations are run with the constant jet in time accurate mode. Animations of this "transition" phase showed no flow changes, thus at the given grid level the flow is steady with the constant pressure jet. The final stage of the solution is to start the oscillating total pressure jet, by setting `ifun=0` (any invalid value, such as -1, has the effect of turning oscillation off).

Jet total temperature was set to double of that of the free-stream and pressure was allowed to oscillate from approximately p_{t_∞} to $\frac{4}{3}p_{t_\infty}$. Sample T_t and p_t contour plots are shown at the initial condition, Figure 8 and maximum and minimum p_t points in the developed oscillatory jet flow, Figures 9 and 10 respectively. Flow field animations are included in the delivered CD-ROM.

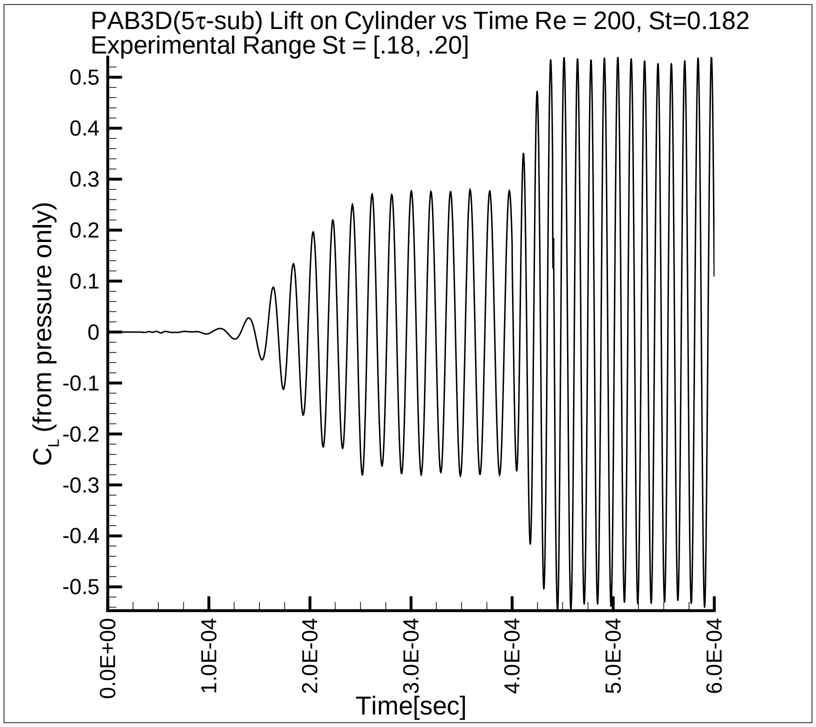

Figure 4: Circular Cylinder: C_L history, second-order time accurate, with five duel time iterations

5 Concluding Remarks

PAB3D's time accurate capabilities have been successfully upgraded to second-order time accuracy using two proven approaches, physical time sub-iteration and duel time sub-iteration. Comparisons with experimental data indicate both methods are accurate. It should be noted that for an equal sized time step and number of iterations per time level, the physical time iteration scheme will always have less error than the duel time scheme. The purpose of duel time stepping is to enable the use of a larger time step than would normally be allowed by stability. Thus, the real advantage of duel time stepping is for higher Reynolds number problems. Also, care must be used to determine the number of iterations required at each time level. The only sure way to do this is run multiple trials and perform a time iteration sensitivity analysis.

In addition to the new time integration schemes, oscillatory jet boundary conditions for total pressure and velocity have been implemented and demonstrated for total pressure oscillation. User customize-able shell functions for total pressure and velocity boundary conditions have been added and documented. The functions performed well and are suitable for production runs. All data and post processing files and scripts are included in the deliverables on CD-ROM.

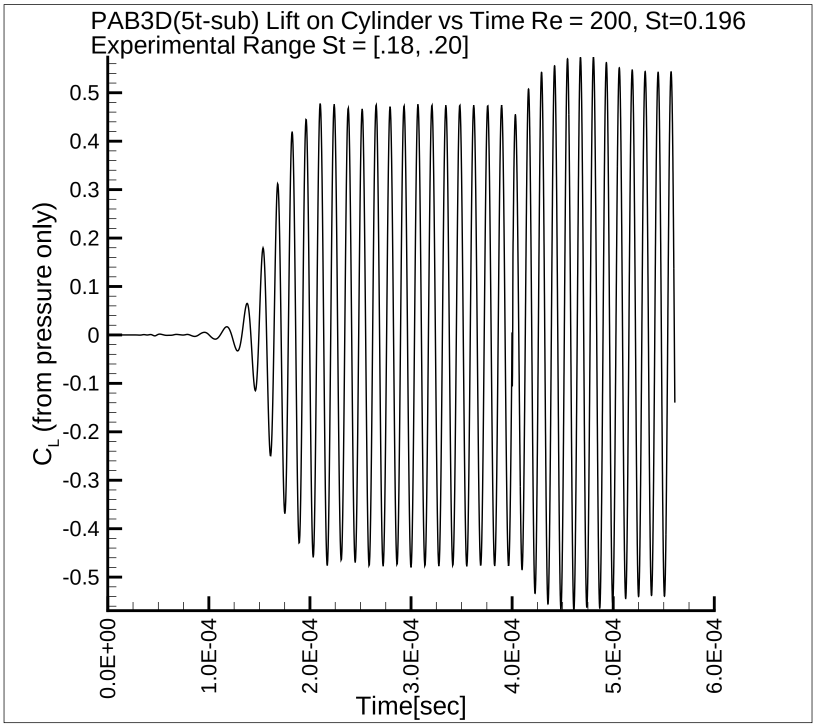

Figure 5: Circular Cylinder: C_L history, second-order time accurate, with physical time iterations

6 Acknowledgments

The authors wish to thank Craig Hunter and Karen Deere of the Configuration Aerodynamics Branch of LaRC for their helpful input and for the contribution of the cylinder grid.

References

[1] Pulliam, T., "Time Accuracy and the Use of Implicit Methods," AIAA Paper 93-3360, 1993.

[2] Jameson, A., "Time Dependent Calculations Using Multigrid with Applications to Unsteady Flows Past Airfoils and Wings," AIAA Paper 91-1595, 1991.

[3] Rumsey, C., Sanetrick, M., Biedron, R., Melson, D., and Parlette, E., "Efficiency and Accuracy of Time-Accurate Turbulent Navier-Stokes Computations," AIAA Paper 95-1835, 1995.

[4] Morkovin, M., "Flow Around a Circular Cylinder - A Kaleidoscope of Challenging Fluid Phenomena," Asme symposium on fully separated flows, 1964.

[5] Roshko, A., "Experimental on Flow Past a Circular Cylinder at Very High Reynolds Number," *Journal of Fluid Mechanics*, Vol. 10, No. 2, 1961, pp. 345–356.

[6] Schlichting, H., *Boundary-Layer Theory*, McGraw-Hill, New York, 1979.

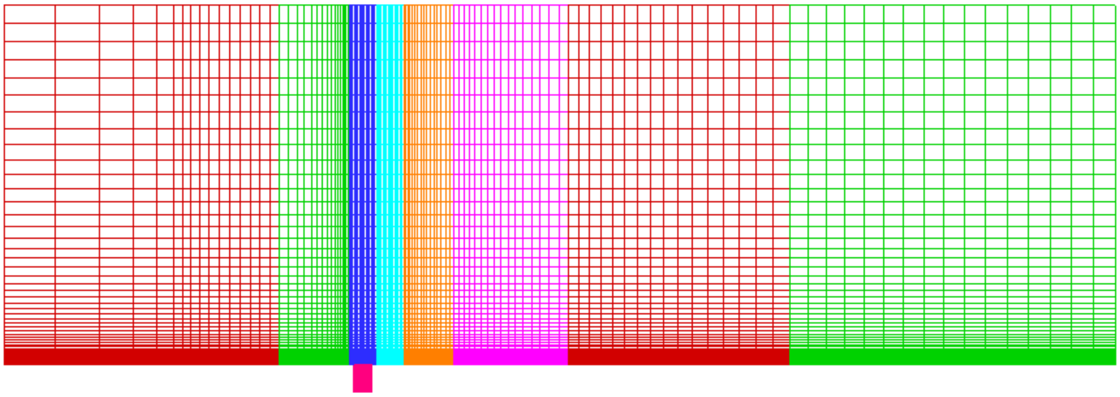

Figure 6: Oscillating Jet: Symmetry plane grid

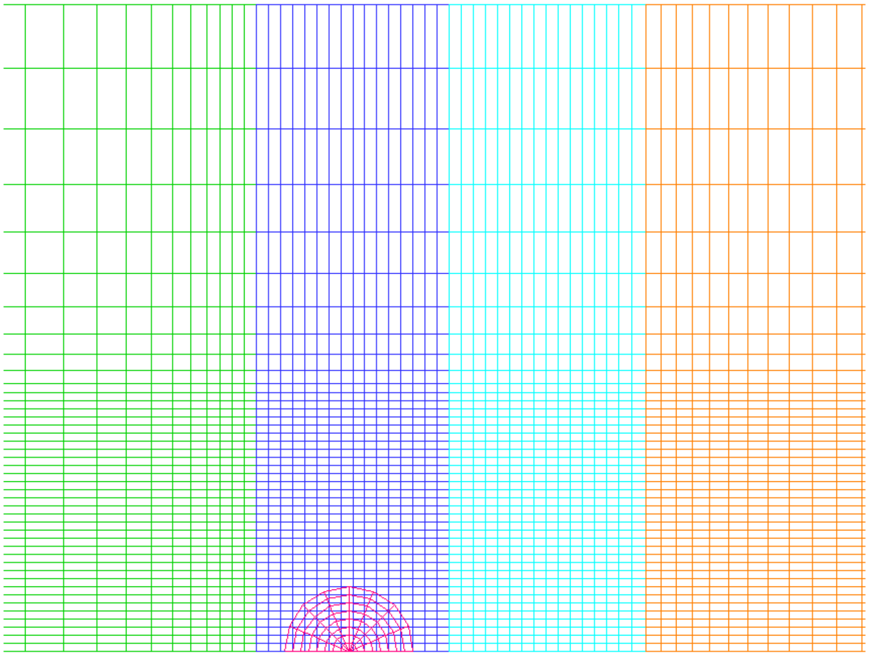

Figure 7: Oscillating Jet: Close-up of jet interface grid

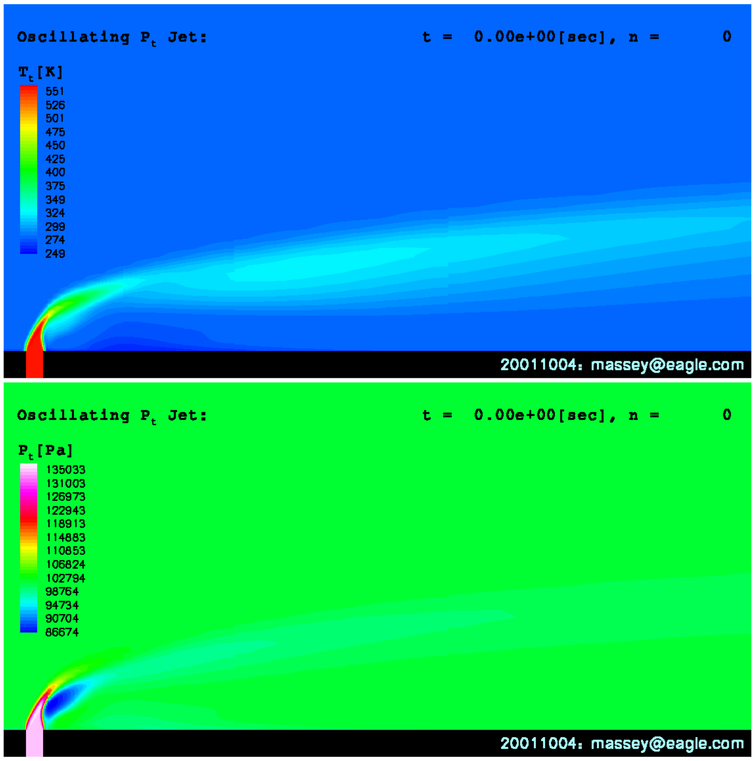

Figure 8: Oscillating Jet: Total temperature and total pressure contours for initial condition.

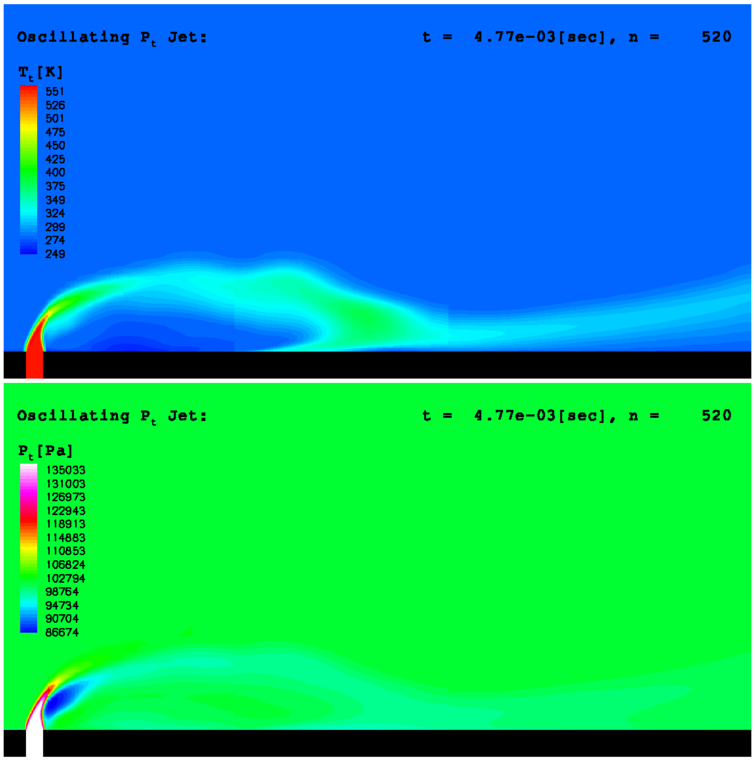

Figure 9: Oscillating Jet: Total temperature and total pressure contours near p_t max

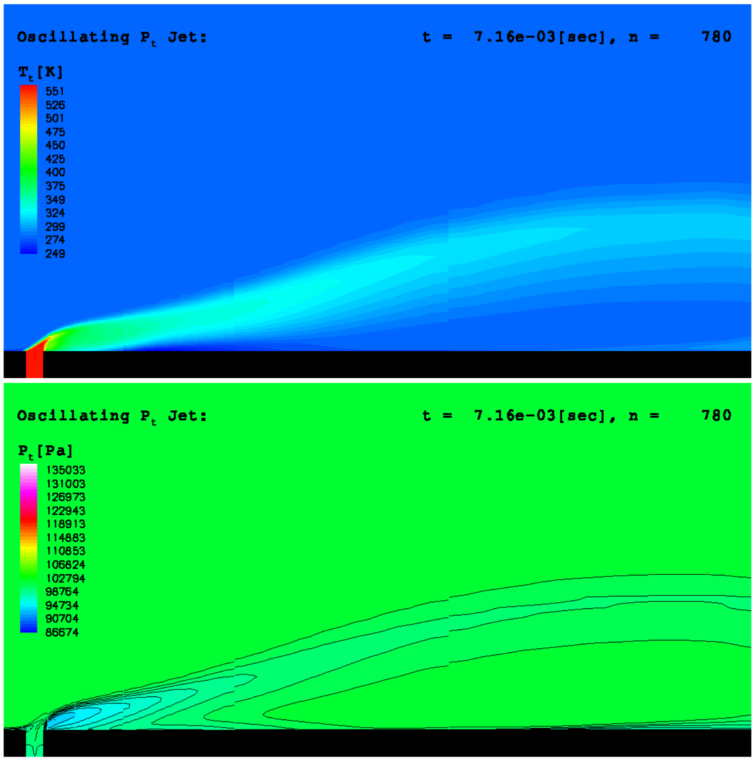

Figure 10: Oscillating Jet: Total temperature and total pressure contours near p_t min